Simulations of Li ion diffusion in the electrolyte material – Li_3PO_4 [a, b]

N. A. W. Holzwarth
Wake Forest University, Winston-Salem, NC, USA

- Motivation
- Calculational methods
- Diffusion in crystalline material
- Oxygen and nitrogen defect structures

---

[a] This work was done in collaboration with Dr. Yaojun Du
[b] Supported by NSF DMR-0405456 and DMR-0427055

Diagram of discharge operation for a Li-ion battery

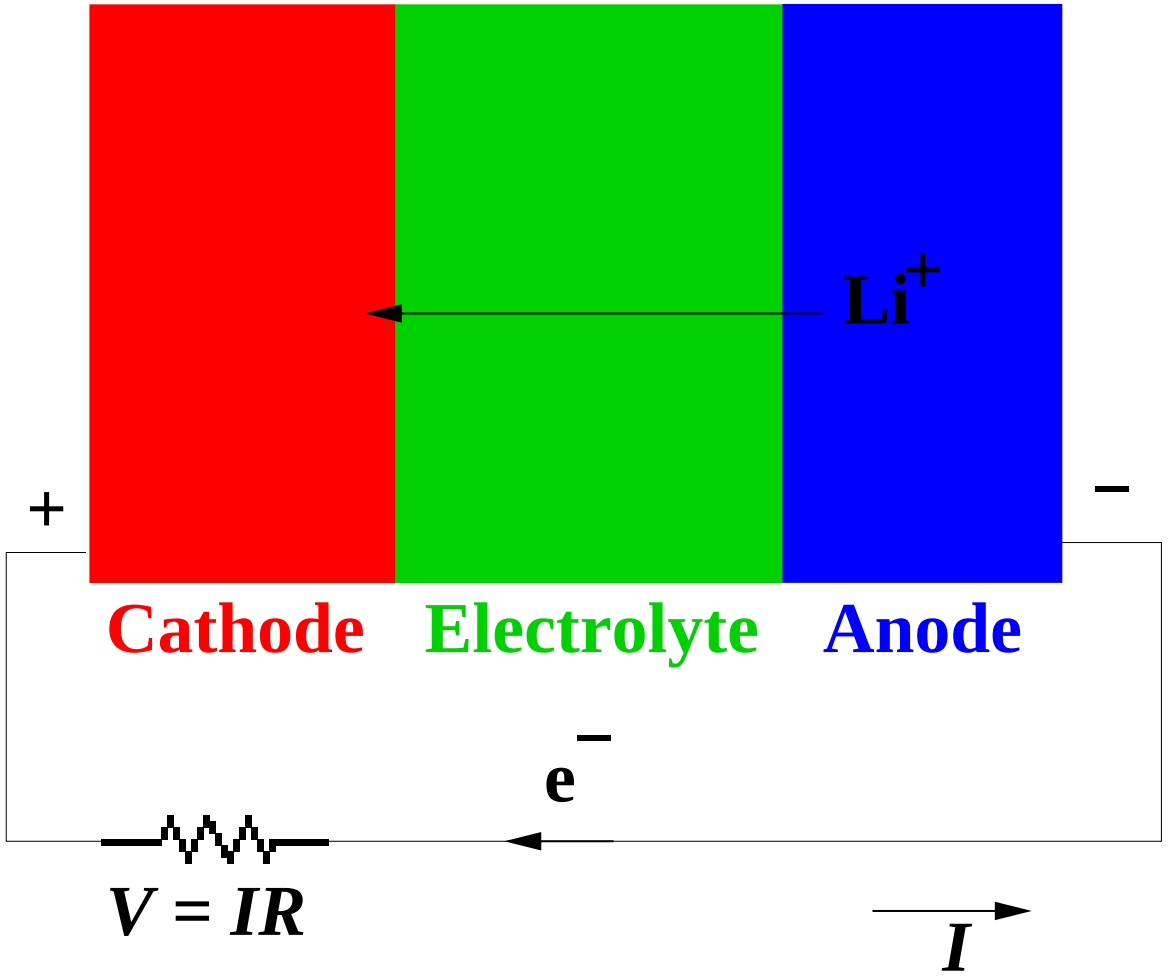

LiPON (Li_3PO_4 + N) developed at ORNL

Journal of Power Sources, 43–44 (1993) 103–110

Fabrication and characterization of amorphous lithium electrolyte thin films and rechargeable thin-film batteries

J. B. Bates, N. J. Dudney, G. R. Gruzalski, R. A. Zuhr, A. Choudhury and C. F. Luck
Oak Ridge National Laboratory, Oak Ridge, TN 37830 (USA)
J. D. Robertson
Department of Chemistry, University of Kentucky, Lexington, KY 40506 (USA)

Abstract

Amorphous oxide and oxynitride lithium electrolyte thin films were synthesized by r.f. magnetron sputtering of lithium silicates and lithium phosphates in Ar, $Ar+O_2$, $Ar+N_2$, or N_2. The composition, structure, and electrical properties of the films were characterized using ion and electron beam, X-ray, optical, photoelectron, and a.c. impedance techniques. For the lithium phosphosilicate films, lithium ion conductivities as high as 1.4×10^{-6} S/cm at 25 °C were observed, but none of these films selected for extended testing were stable in contact with lithium. On the other hand, a new thin-film lithium phosphorus oxynitride electrolyte, synthesized by sputtering Li_3PO_4 in pure N_2, was found to have a conductivity of 2×10^{-6} S/cm at 25 °C and excellent long-term stability in contact with lithium. Thin-films cells consisting of a 1 μm thick amorphous V_2O_5 cathode, a 1 μm thick oxynitride electrolyte film, and a 5 μm thick lithium anode were cycled between 3.7 and 1.5 V using discharge rates of up to 100 $\mu A/cm^2$ and charge rates of up to 20 $\mu A/cm^2$. The open-circuit voltage of 3.6 to 3.7 V of fully-charged cells remained virtually unchanged after months of storage.

Properties

- Chemical and structural stability.
- Reasonable Li^+ conductivity.
- Stable contacts with anodes and cathodes.

Questions

1. What is the basic mechanism for Li^+ transport in crystalline Li_3PO_4?
   - Migration of Li^+ vacancies?
   - Migration of Li^+ interstitials?
2. What are the effects of O and N defects? Neutral materials have stoichiometries: $Li_{3+x}PO_{4-y}N_z$, with $x = 3z - 2y$.
   - Stable defect structures.
   - Effects on Li^+ migration.

Summary of "first-principles" calculational methods

Basic approximations

- All calculations are carried out using supercells composed of 16 Li_3PO_4 units.
- Nuclear motions are assumed to be separable from the electronic motions within the Born-Oppenheimer approximation and are treated classically.
- Electronic effects are treated within density functional theory (DFT) using the local density approximation (LDA) form of the exchange-correlation functional. (A few results were obtained using the generalized gradient approximation (GGA) form.) These calculations give us the total energies corresponding to the electronic ground state $E(\{\mathbf{R}^a\})$ corresponding to the nuclear coordinates $\{\mathbf{R}^a\}$ and with corresponding self-consistent electron density $\rho(\mathbf{r}, \{\mathbf{R}^a\})$.
- Meta-stable configurations are determined by minimizing the total energies and converging the forces ($|\nabla_a E(\{\mathbf{R}^a\})| < 0.01$ eV/Å).
- Migration energies E_m between adjacent metal-stable configurations are determined using the Nudged Elastic Band method within an estimated error of ± 0.05 eV.

Codes for electronic structure calculations

Method	Comments
PAW *pwpaw* - pwpaw.wfu.edu *socorro* - dft.sandia.gov/socorro *abinit* - www.abinit.org	Works well for moderately large unit cells, but variable unit cell optimization not yet implemented in *pwpaw* and *socorro*. Need to construct and test PAW basis and projector functions.
LAPW *wien2k* - www.wien2k.at	Works well for smaller unit cells; variable unit cell optimization not implemented. Need to choose non-overlapping muffin tin radii and avoid "ghost" solutions.
PWscf *pwscf* - www.pwscf.org	Works well for large unit cells and includes variable unit cell optimization. Need to construct and test soft pseudopotential functions.

Secret recipe for pseudopotential construction

	r_c (bohr)	Atomic basis
Li		
PAW*	1.61	$1s, 2s, 2p$
PWscf†	1.60	$1s, 2s, 2p$
LAPW	1.70	$1s, \epsilon s, \epsilon p$
O		
PAW*	1.41	$2s, \epsilon s, 2p, \epsilon p$
PWscf†	1.40	$2s, \epsilon s, 2p, \epsilon p$
LAPW	1.28	$2s, \epsilon s, \epsilon p$
P		
PAW*	1.51	$2s, 3s, 2p, 3p$
PWscf†	1.50	$3s, \epsilon s, 3p, \epsilon p, \epsilon d$
LAPW	1.38	$\epsilon s, 2p, \epsilon p$

* PAW basis and projector functions generated by *atompaw* code.

† Ultra-soft pseudopotentials generated by *uspp* code of David Vanderbilt.

Test results for simple oxides

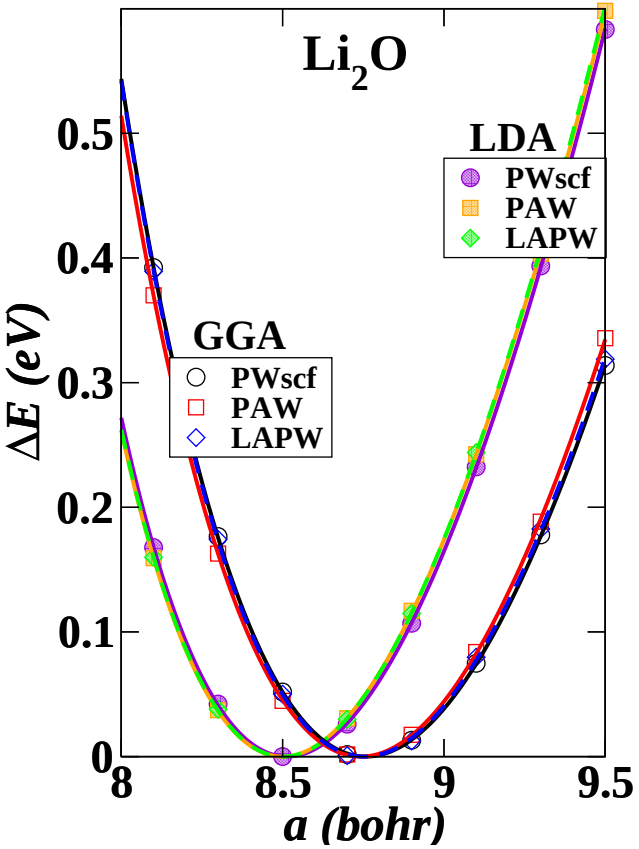

Fluorite structure

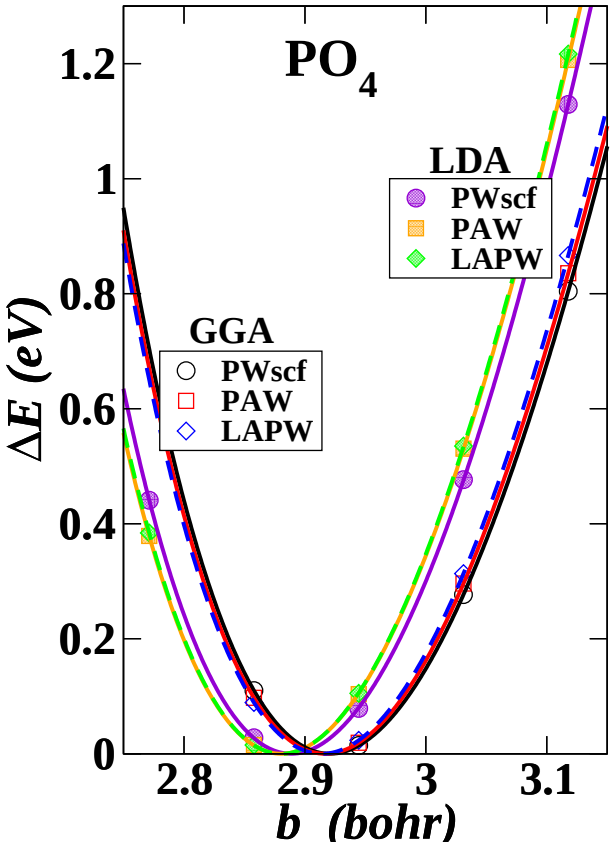

Tetrahedral molecule

Validation of calculations – comparison with Raman spectral data

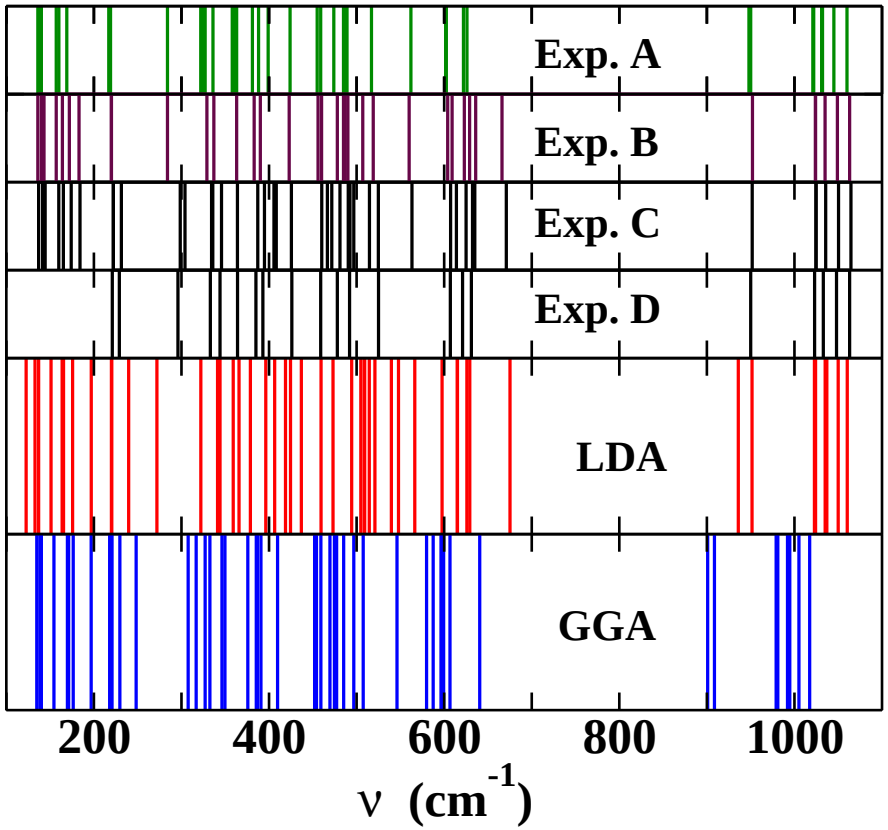

γ-Li_3PO_4

Exp. A – (RT) – Mavrin & co-workers, *JETP* **96**, 53 (2003); Exp. B – (RT) – Harbach & co-workers, *Phys. Stat. Sol. B* **66**, 237 (1974); Exp. C – (LNT) – Harbach; Exp. D – (LNT) Popović & co-workers, *J. Raman Spec.* **34** 77, (2003)

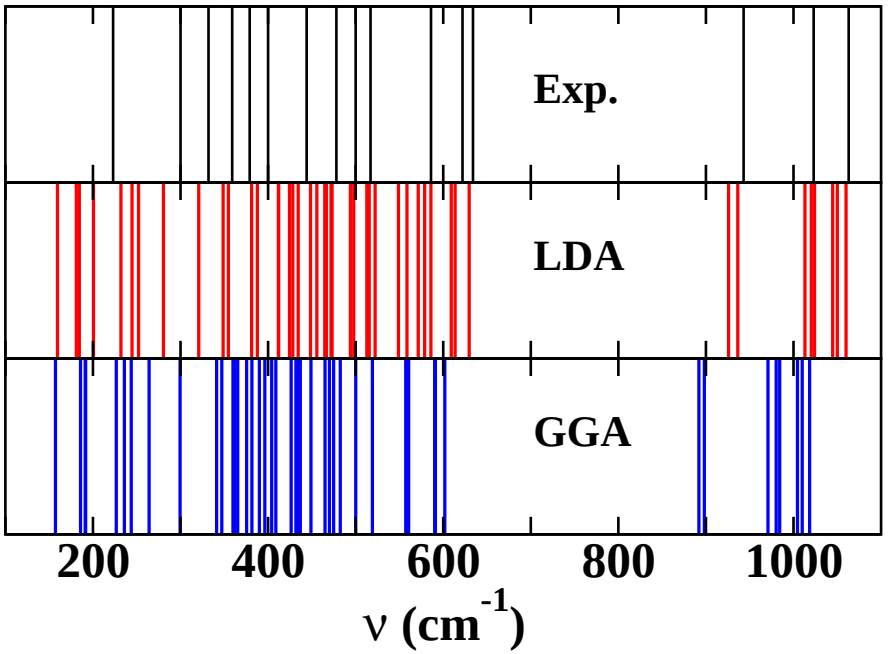

β-Li_3PO_4

Exp. – (LNT) Popović & co-workers, *J. Raman Spec.* **34** 77, (2003)

Ionic conductivity via activated hopping

Schematic diagram of minimal energy path

Approximated using NEB algorithm[a]
– "Nudged Elastic Band"

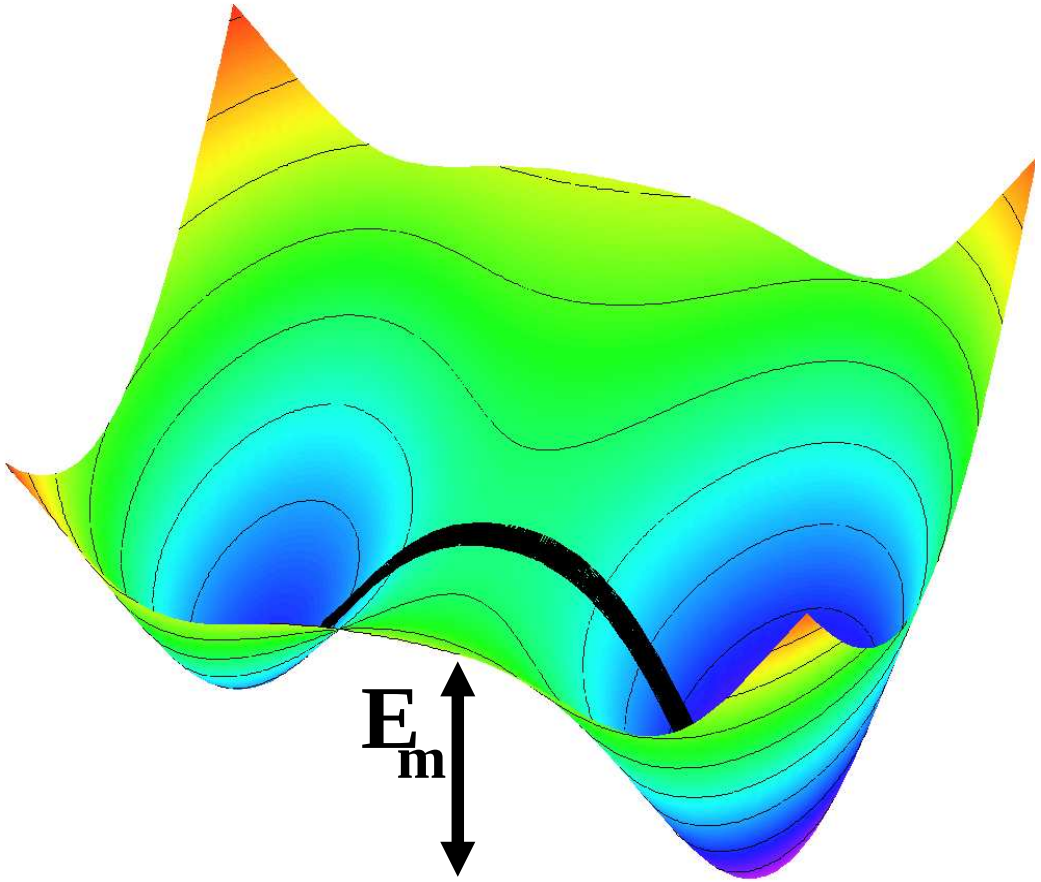

[a] Henkelman and Jónsson, *JCP* **113**, 9978 (2000)

Arrhenius relation

$$\sigma \cdot T = K \mathrm{e}^{-E_A/kT}$$

From: Ivanov-Shitz and co-workers,
Cryst. Reports **46**, 864 (2001):

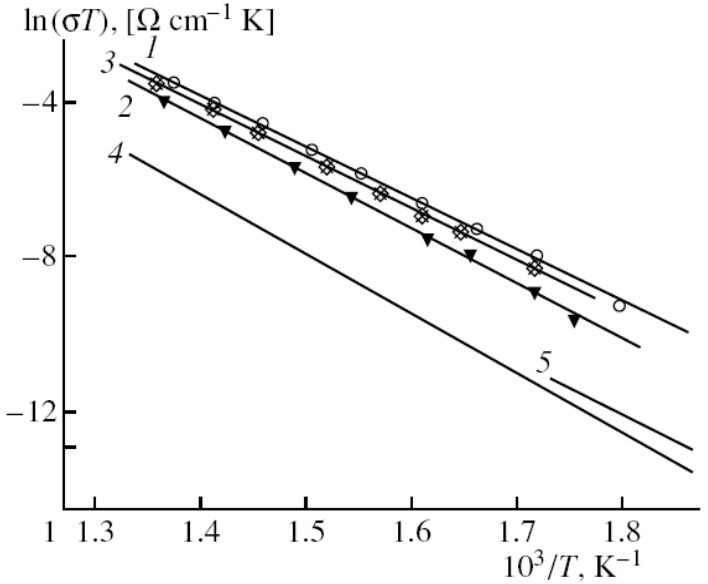

Fig. 2. Temperature dependences of conductivity in γ-Li_3PO_4: (*1–3*) for single crystals measured along the (*1*) *a*-axis, (*2*) *b*-axis, (*3*) *c*-axis and (*4, 5*) for a polycrystal (*4*) according to [4, 5] and (*5*) according to [7].

E_A = 1.14, 1.23, 1.14, 1.31, 1.24 eV for 1,2,3,4,5, respectively.

Crystalline Li_3PO_4

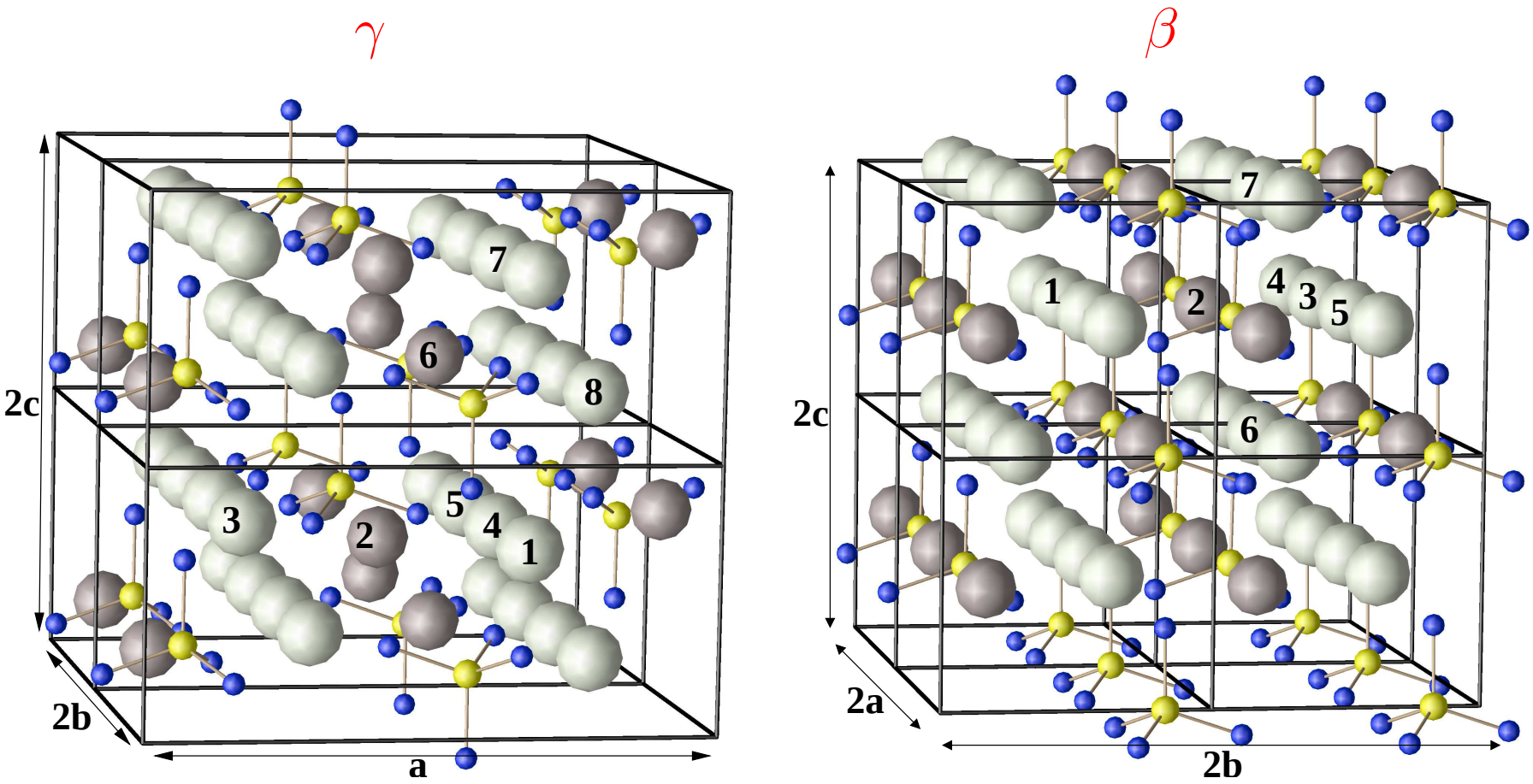

Ball and stick drawing of the equilibrium structures of the γ-Li_3PO_4 and β-Li_3PO_4 supercells used in the simulations. The PO_4 groups are indicated with bonded yellow and blue spheres. Li ions are indicated by light and dark gray spheres representing the crystallographically distinct sites. The number labels on some of the Li sites are used to describe vacancy diffusion.

Example of configuration coordinate diagrams for vacancy diffusion in Li_3PO_4

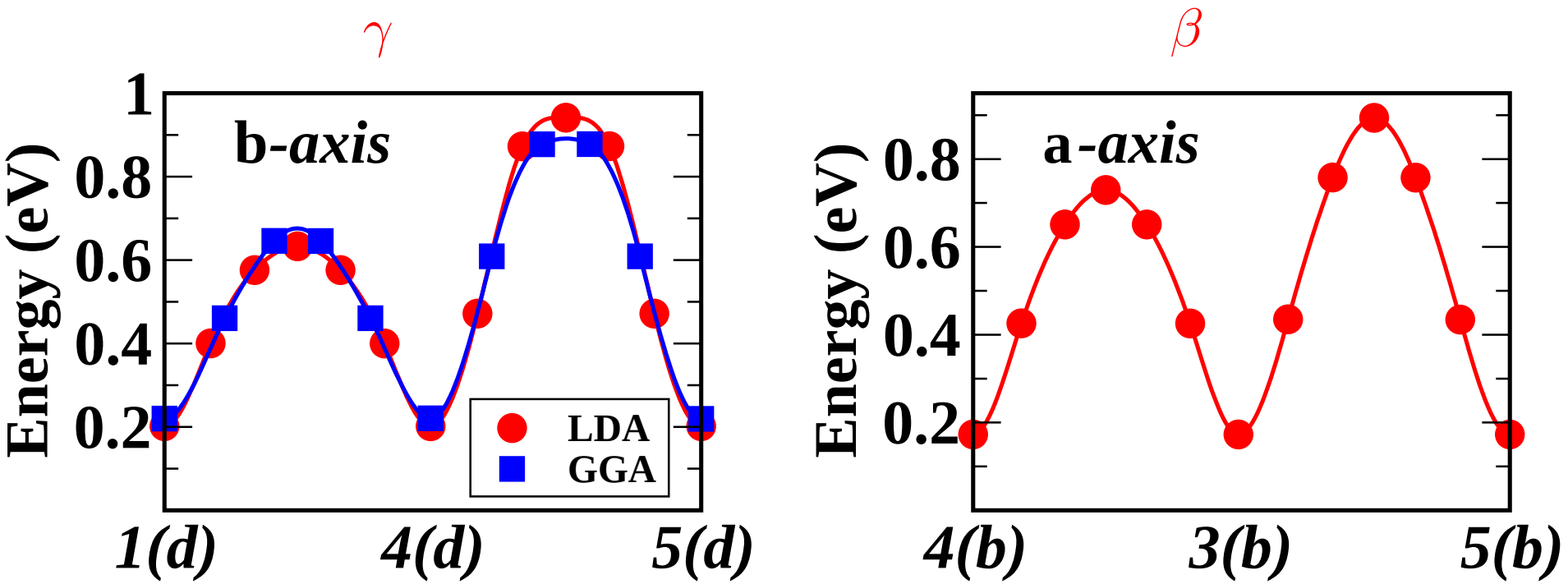

Summary of vacancy diffusion steps in γ-Li_3PO_4 and β-Li_3PO_4.

Axis	Step	Distance (Å)	E_m (eV)
	γ-Li_3PO_4		
a	$1(d) \leftrightarrow 2(c)$	2.91	0.43
	$2(c) \leftrightarrow 3(d)$	3.10	0.66
	$1(d) \leftrightarrow 2(c) \leftrightarrow 3(d)$	5.19	0.66
b	$1(d) \leftrightarrow 4(d)$	2.98	0.43
	$4(d) \leftrightarrow 5(d)$	3.03	0.74
	$1(d) \leftrightarrow 4(d) \leftrightarrow 5(d)$	6.01	0.74
c	$4(d) \leftrightarrow 8(d)$	2.97	0.62
	$4(d) \leftrightarrow 8(d) \leftrightarrow 7(d)$	4.84	0.62
	$4(d) \leftrightarrow 6(c)$	3.41	0.57
	$6(c) \leftrightarrow 7(d)$	2.60	0.68
	$4(d) \leftrightarrow 6(c) \leftrightarrow 7(d)$	4.84	0.68

Axis	Step	Distance (Å)	E_m (eV)
	β-Li_3PO_4		
b	$1(b) \leftrightarrow 2(a)$	2.94	0.51
	$2(a) \leftrightarrow 3(b)$	3.03	0.55
	$1(b) \leftrightarrow 2(a) \leftrightarrow 3(b)$	5.15	0.55
a	$4(b) \leftrightarrow 3(b)$	2.97	0.56
	$3(b) \leftrightarrow 5(b)$	3.04	0.72
	$4(b) \leftrightarrow 3(b) \leftrightarrow 5(b)$	6.01	0.72
c	$6(b) \leftrightarrow 5(b)$	2.96	0.71
	$6(b) \leftrightarrow 5(b) \leftrightarrow 7(b)$	4.76	0.71
	$6(b) \leftrightarrow 2(a)$	2.93	0.71
	$2(a) \leftrightarrow 7(b)$	2.94	0.61
	$6(b) \leftrightarrow 2(a) \leftrightarrow 7(b)$	4.76	0.71

Metastable interstitial Li^+ configurations in γ-Li_3PO_4

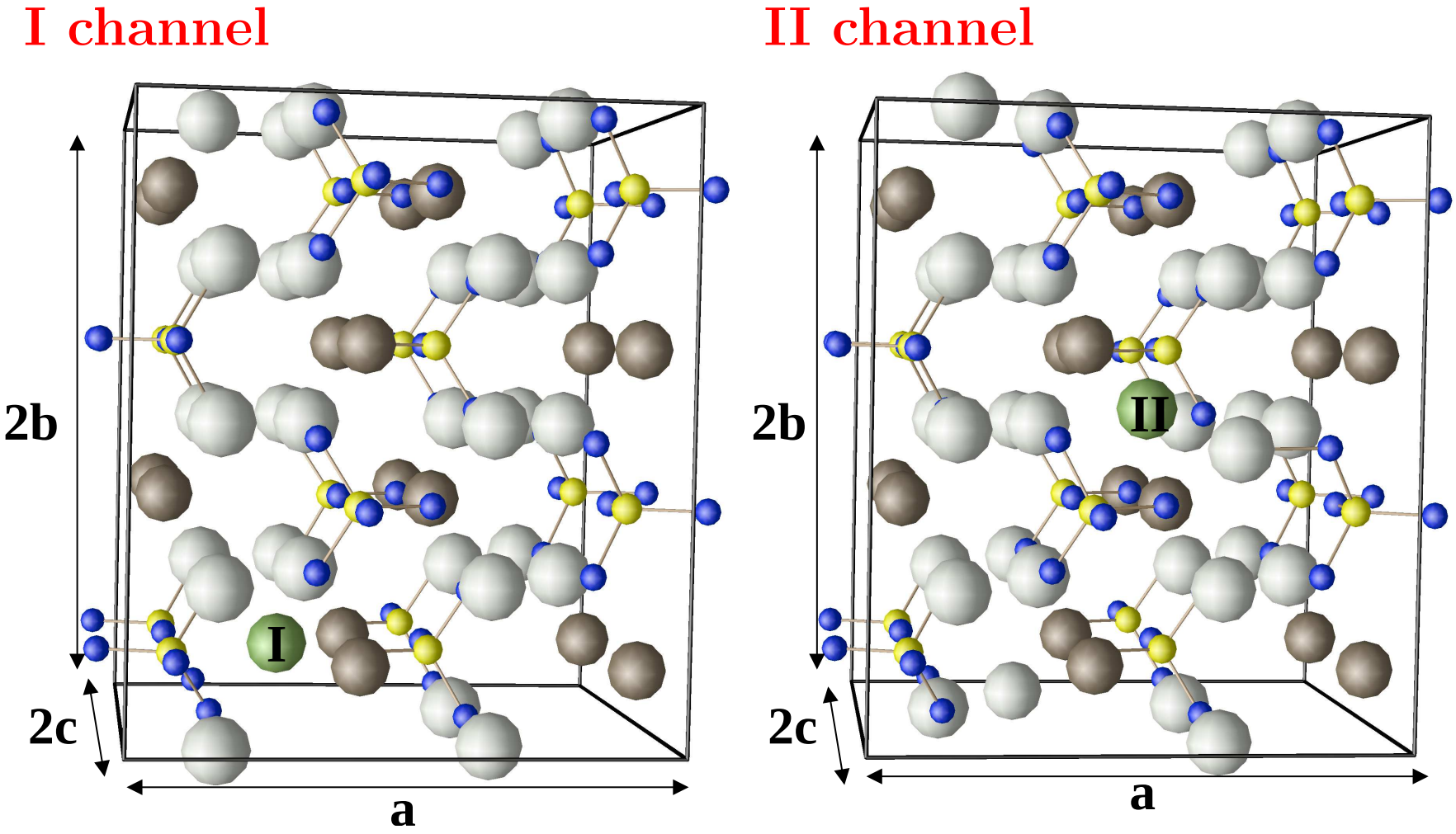

Ball and stick drawing of the metastable interstitial Li^+ sites (indicated with green balls) in γ-Li_3PO_4. Similar structures occur in β-Li_3PO_4.

Example of configuration coordinate diagrams for interstitial diffusion in Li_3PO_4

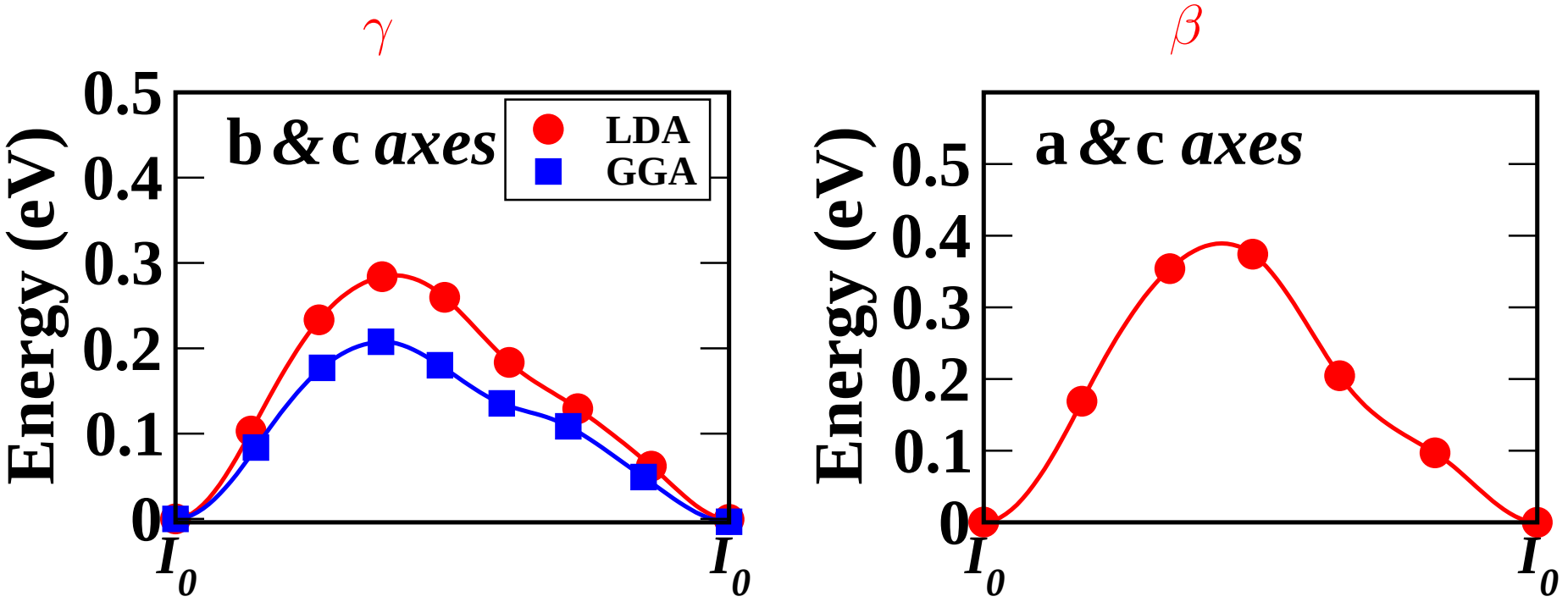

Summary of interstitial diffusion steps in γ-Li_3PO_4 and β-Li_3PO_4.

Type	Step	Distance (Å)	E_m (eV)
γ-Li_3PO_4			
interstitialcy	$I_0 \leftrightarrow I_0$	4.0	0.29
interstitialcy	$I_0 \leftrightarrow II_0$	3.3	0.30
direct hop	$II_0 \leftrightarrow II^*$	0.5	0.14
	$I_0 \leftrightarrow II_0 \leftrightarrow II^* \leftrightarrow II_0 \leftrightarrow I_0$	7.0	0.44
β-Li_3PO_4			
interstitialcy	$I_0 \leftrightarrow I_0$	3.9	0.39
interstitialcy	$I_0 \leftrightarrow II_0$	3.5	0.53
direct hop	$II_0 \leftrightarrow II_1$	0.5	0.05
interstitialcy	$II_1 \leftrightarrow I_0$	2.5	0.52
	$I_0 \leftrightarrow II_0 \leftrightarrow II_1 \leftrightarrow I_0$	6.0	0.53

Illustration of interstitialcy mechanism along b & c axes in γ-Li_3PO_4

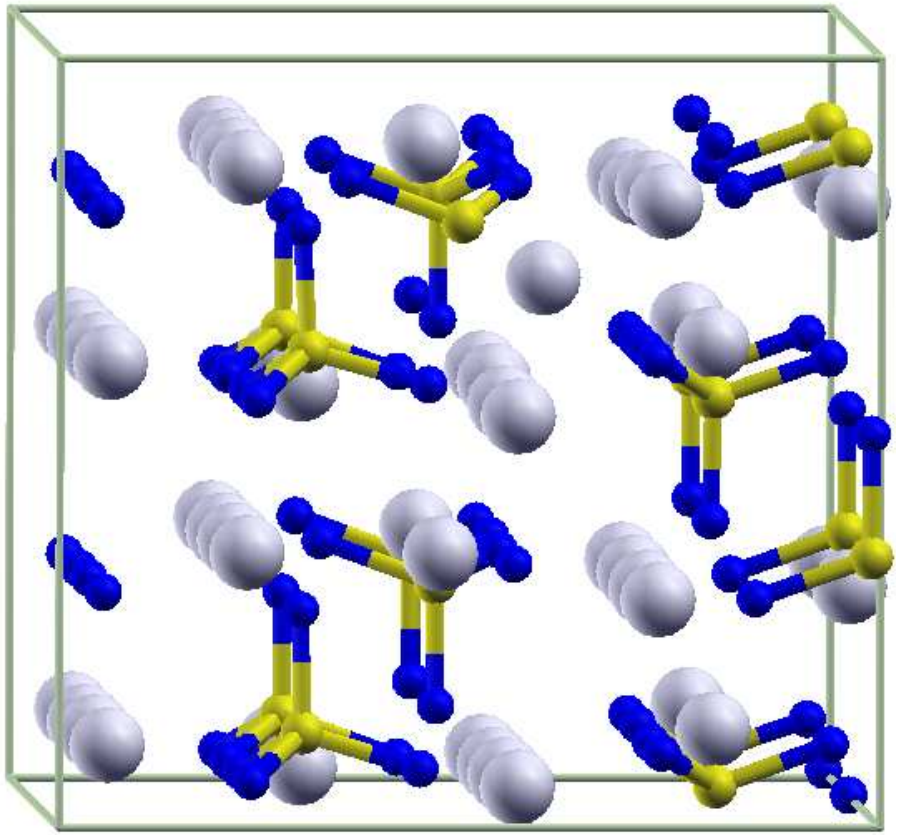

Illustration of interstitialcy mechanism along b & c axes in γ-Li_3PO_4

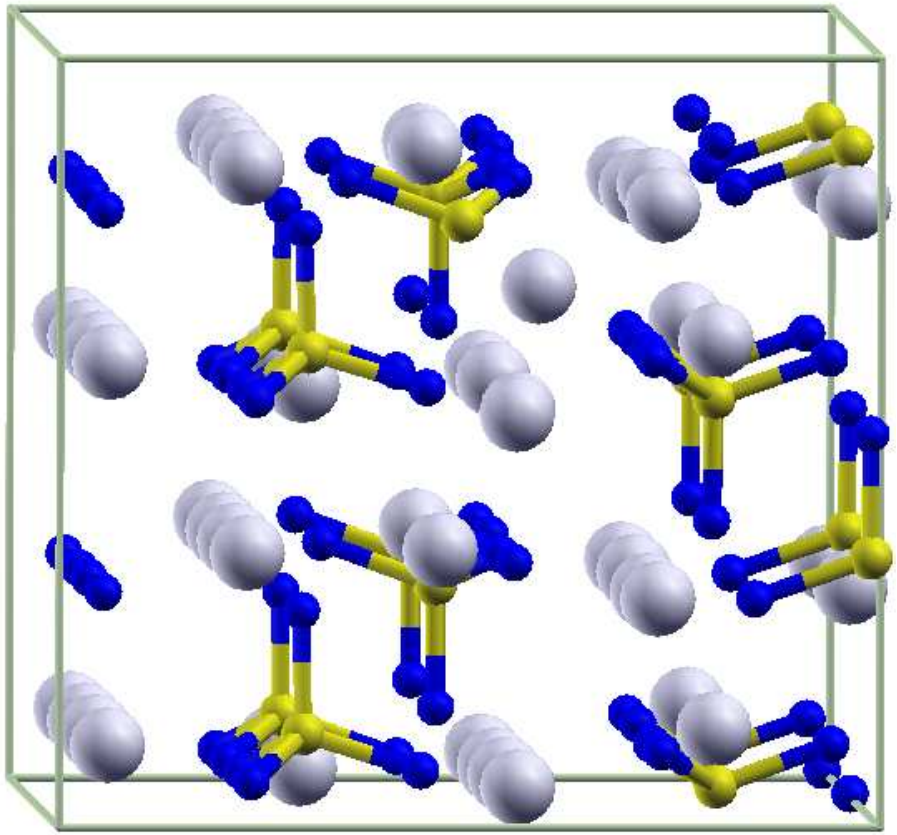

Illustration of interstitialcy mechanism along b & c axes in γ-Li_3PO_4

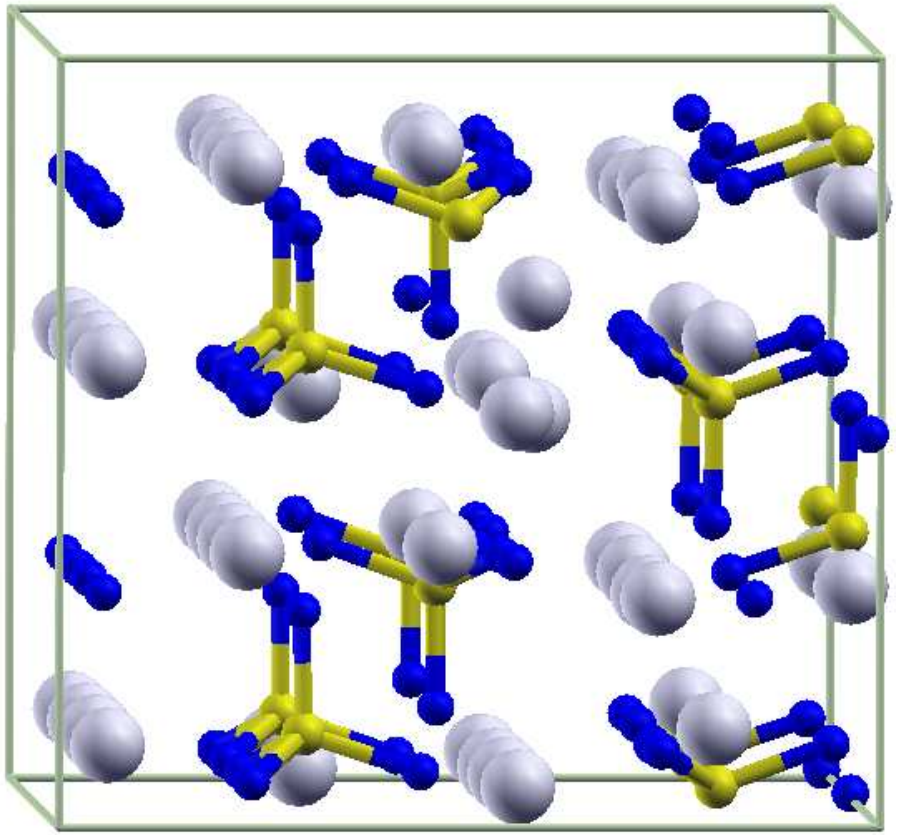

Illustration of interstitialcy mechanism along b & c axes in γ-Li_3PO_4

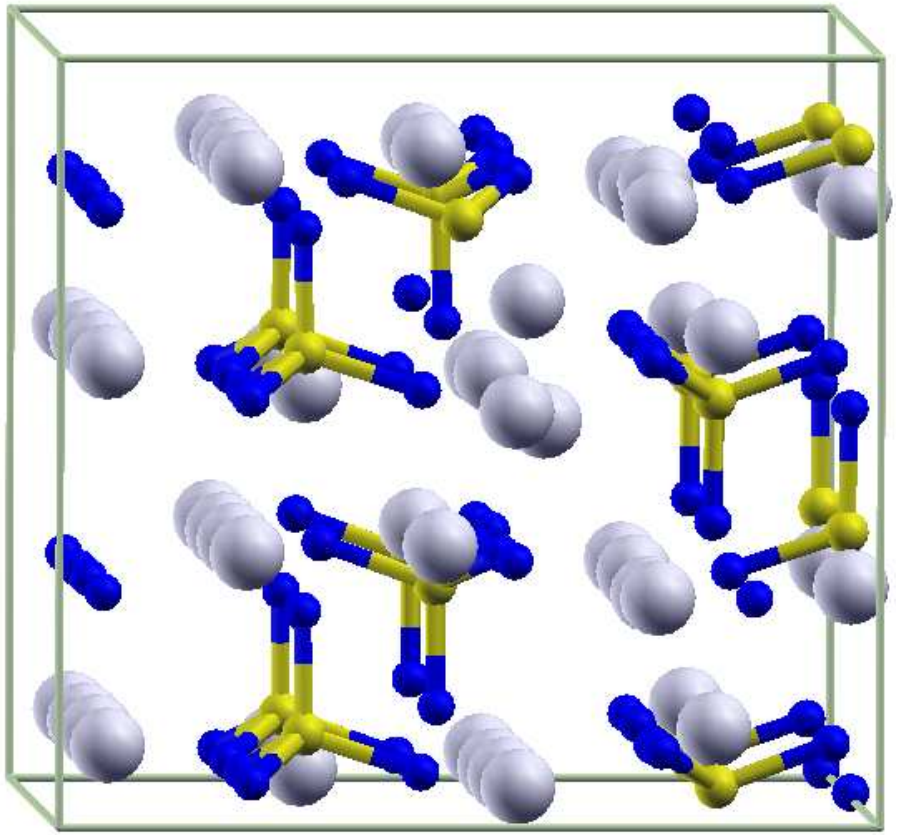

Illustration of interstitialcy mechanism along b & c axes in γ-Li_3PO_4

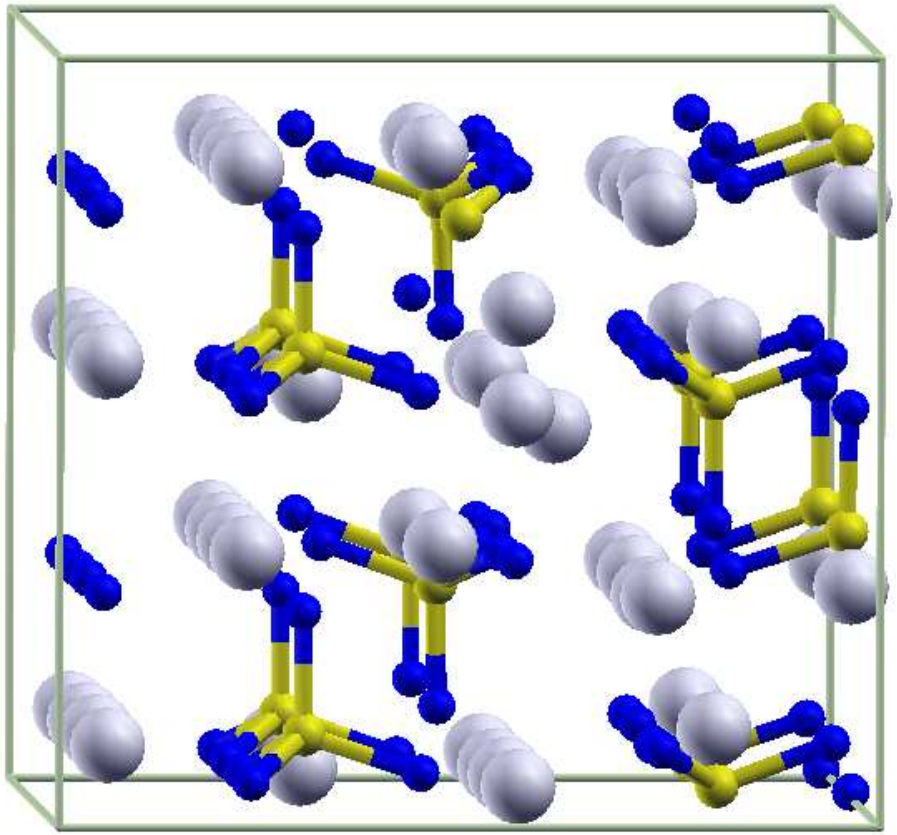

Illustration of interstitialcy mechanism along b & c axes in γ-Li_3PO_4

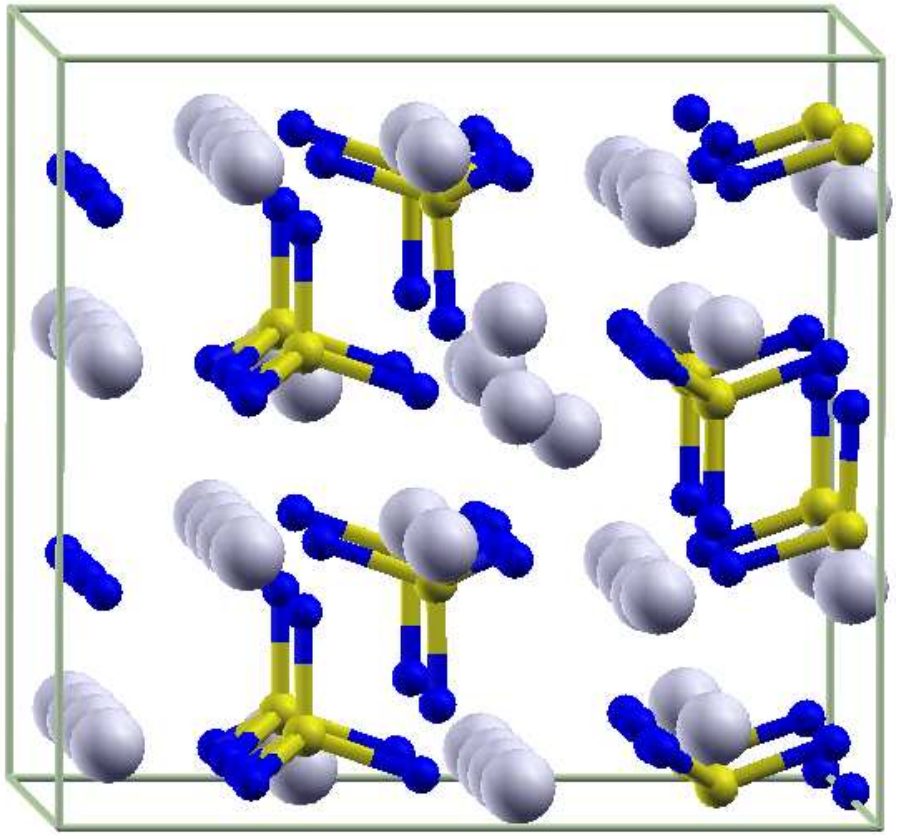

Illustration of interstitialcy mechanism along b & c axes in γ-Li_3PO_4

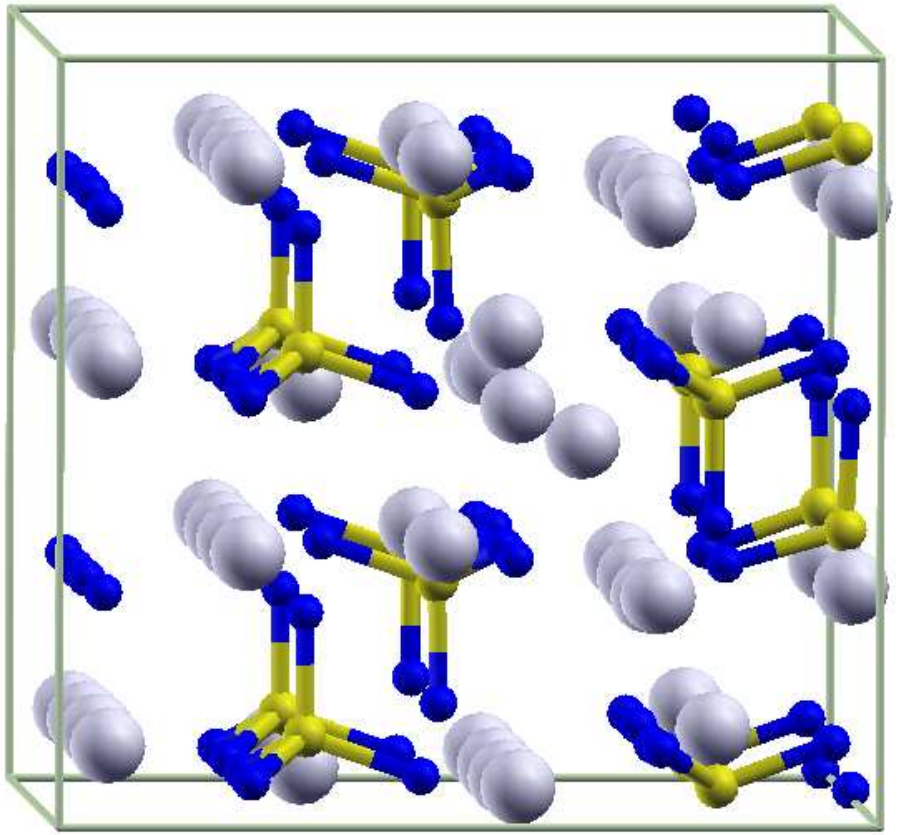

Illustration of interstitialcy mechanism along b & c axes in γ-Li_3PO_4

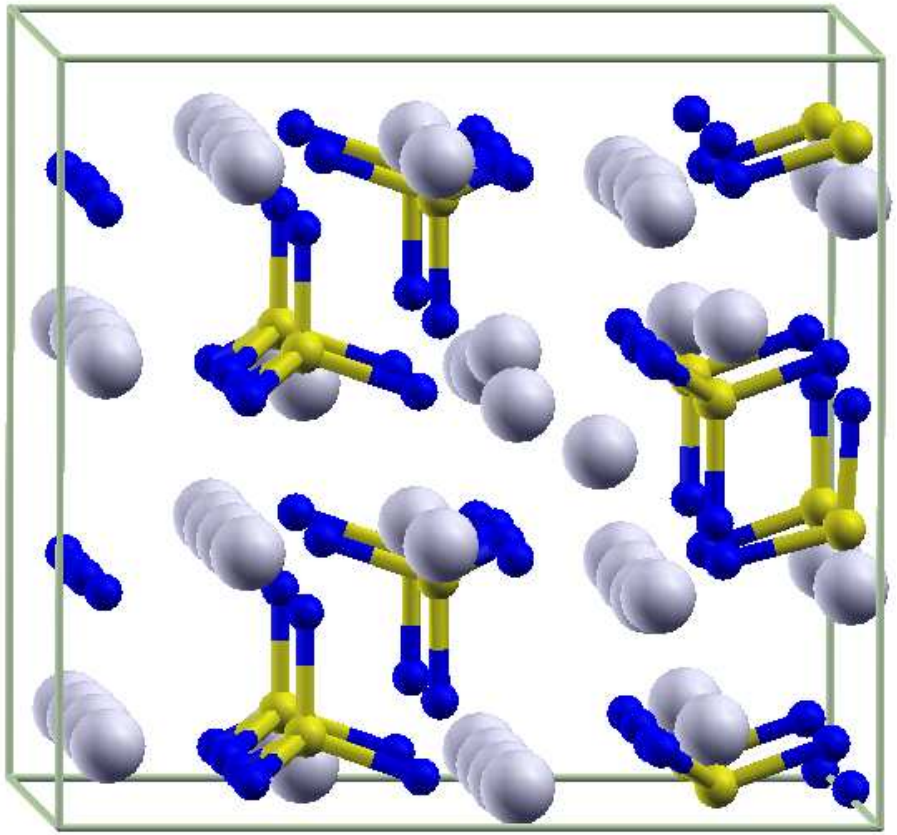

Illustration of interstitialcy mechanism along b & c axes in γ-Li_3PO_4

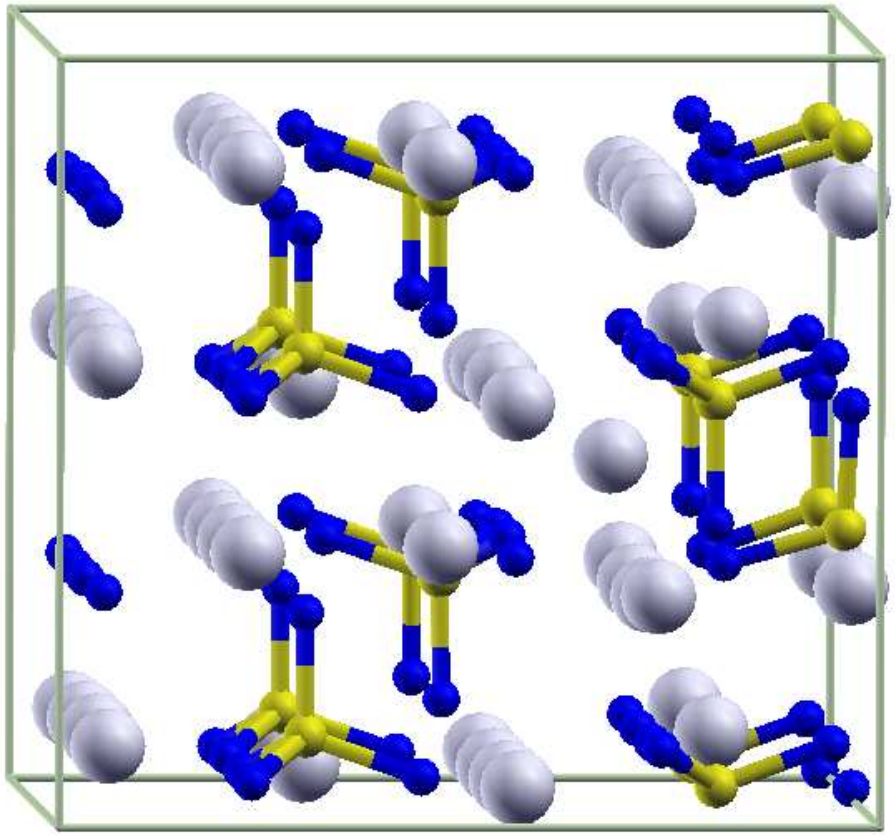

Comparison with experimental measurements of activation energies in crystalline Li_3PO_4

By definition, in a perfect crystal no vacancies or interstitial ions can exist, so that mobile species such as vacancies and interstitials must first be created before ion diffusion can occur. In real crystals, intrinsic defects (vacancy-interstitial pairs) are created thermally with a formation energy E_f and the measured activation energy is given by $\boxed{E_A = E_m + E_f/2}$. Assuming thermal equilibrium between the number of vacancy and interstitial defects compared with the number of unvacant lattice sites and unoccupied interstitial sites, the concentration (n) of vacancies and interstitials is determined by a Boltzmann factor $n^2 \propto \mathrm{e}^{-E_f/kT}$. Thus the Arrhenius equation takes the form

$$\sigma \cdot T = K' \; n\mathrm{e}^{-E_m/kT} \equiv K' \; \mathrm{e}^{-(E_m + E_f/2)/kT}.$$

Estimated minimum migration, formation, and activation energies (in eV) compared with temperature coefficient of ionic conductivity in single crystals (Ivanov-Shitz and co-workers, *Cryst. Reports* **46**, 864 (2001)

Direction	E_f	E_m	E_A	E_A(exp)
γ-Li_3PO_4				
a	1.7	0.44	1.3	1.23
b		0.29	1.1	1.14
c		0.29	1.1	1.14
β-Li_3PO_4				
b	2.1	0.53	1.6	
a		0.39	1.4	
c		0.39	1.4	

Defect structures – γ-$Li_{3-\frac{1}{16}}PO_{4-\frac{2}{16}}N_{\frac{1}{16}}$

Stable "bent" P–N–P structure

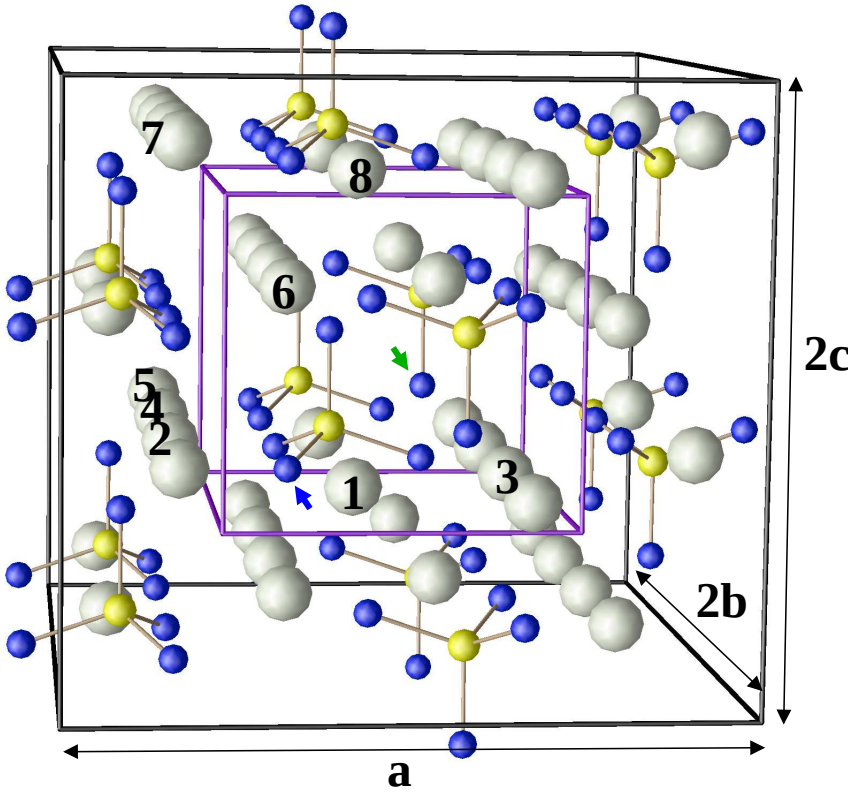

Ideal supercell

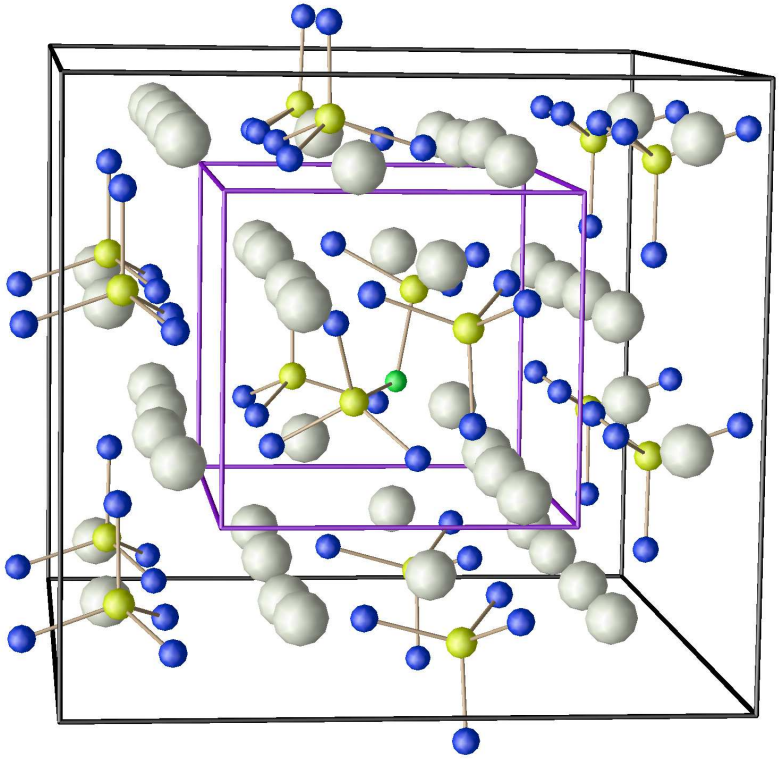

Relaxed structure

Defect structures – γ-$Li_{3-\frac{1}{16}}PO_{4-\frac{2}{16}}N_{\frac{1}{16}}$

Stable "bent" P–N–P and P–O–P structures

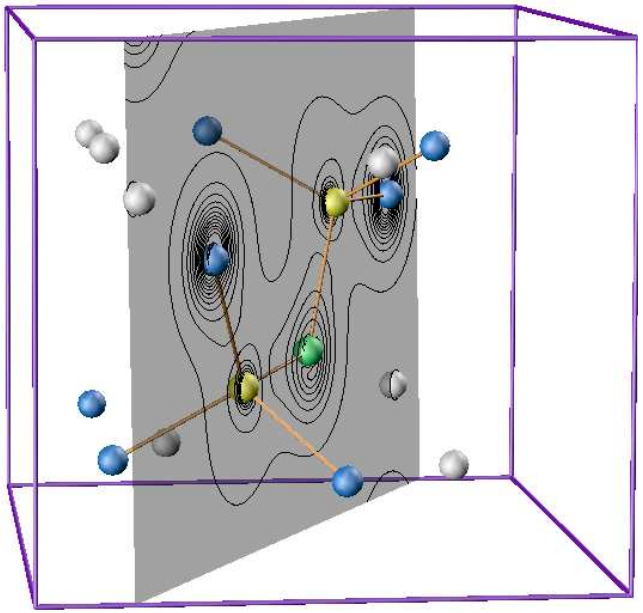

Contours of electron density for "bent" P–N–P structure

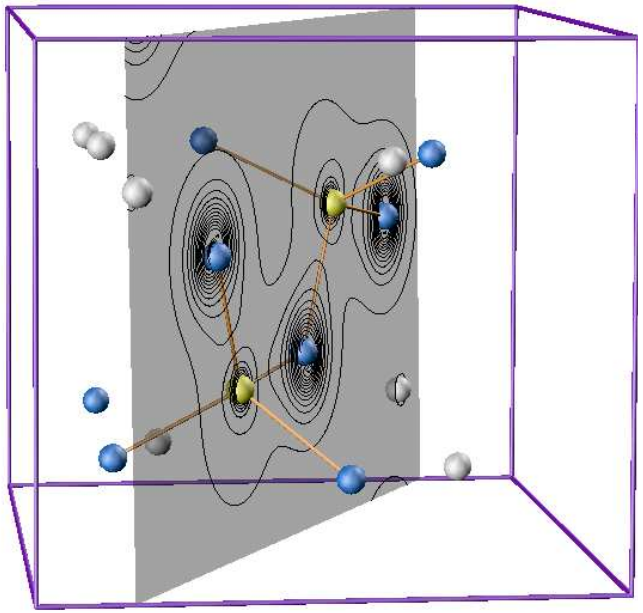

Contours of electron density for "bent" P–O–P structure

Defect structures – γ-$Li_{3-\frac{1}{16}}PO_{4-\frac{2}{16}}N_{\frac{1}{16}}$

Stable "straight" P–N–P structure

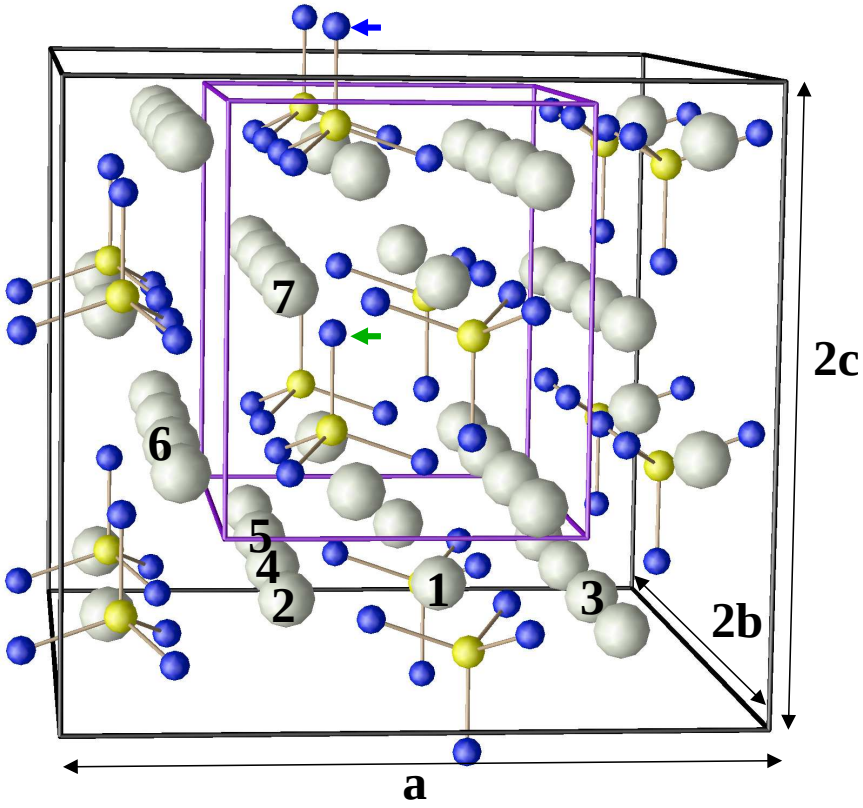

Ideal supercell

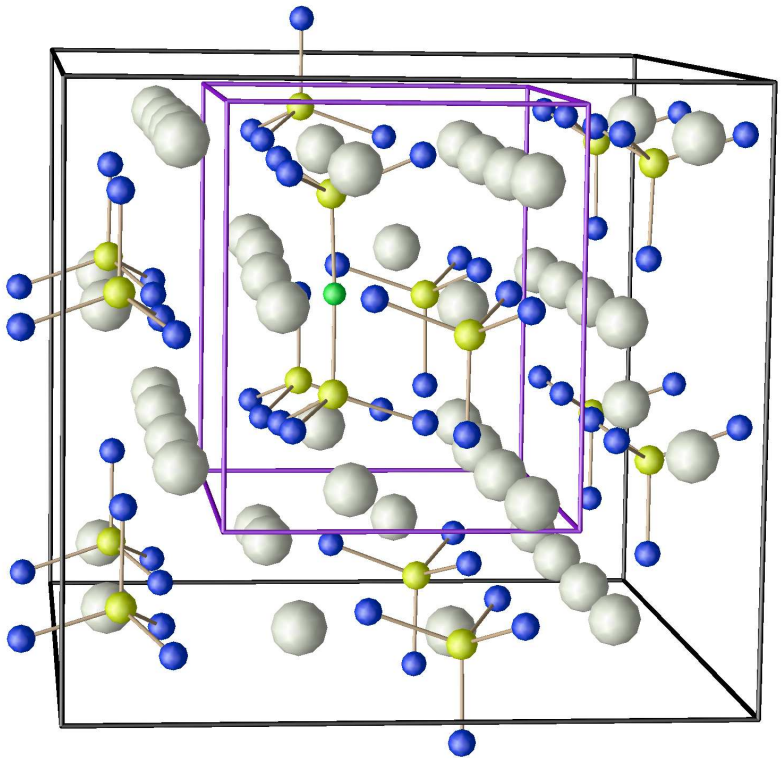

Relaxed structure

Defect structures – γ-$Li_{3-\frac{1}{16}}PO_{4-\frac{2}{16}}N_{\frac{1}{16}}$

Stable "straight" P–N–P and P–O–P structures

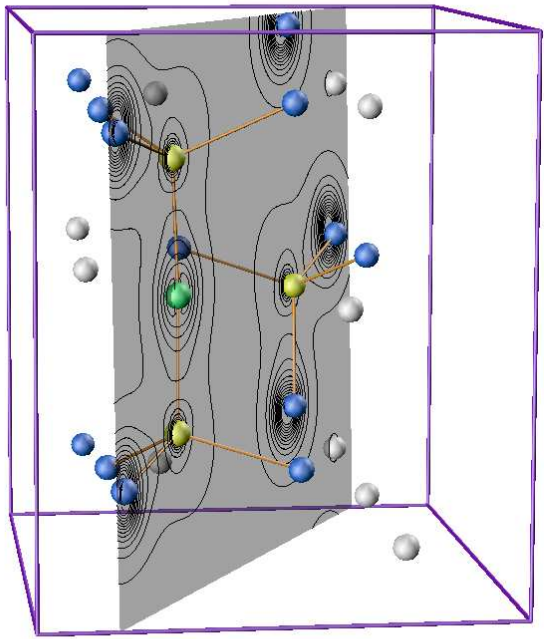

Contours of electron density for "straight" P–N–P structure

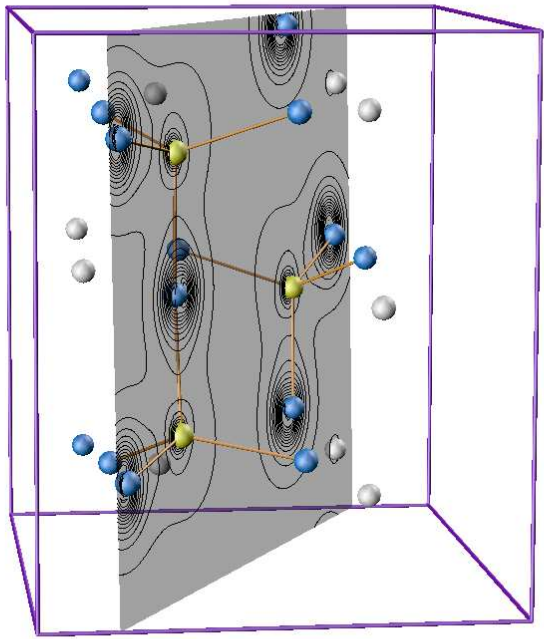

Contours of electron density for "straight" P–O–P structure

Summary of properties of defect structures in γ-Li_3PO_4.

Bond lengths, angles, and relative supercell energies for P−N−P and P−O−P structures.

Type	Bond lengths (Å)*	Bond angle	Energy (eV)
P−N−P (bent)	1.63, 1.66	118(°)	0.00
P−N−P (straight)	1.63, 1.62	174(°)	0.05
P−O−P (bent)	1.66, 1.70	122(°)	2.71
P−O−P (straight)	1.69, 1.66	171(°)	2.59

* For comparison, tetrahedral P−O bonds are calculated to be 1.54-1.57 Å.

Summary

1. What is the basic mechanism for Li^+ transport in crystalline Li_3PO_4?
   - Migration of Li^+ vacancies?
     $\Longrightarrow$ $E_m \approx 0.6 - 0.7$ eV
   - Migration of Li^+ interstitials?
     $\Longrightarrow$ $E_m \approx 0.3 - 0.5$ eV
   - Activation energy for crystalline Li_3PO_4
     $\Longrightarrow$ $E_A = E_m + E_f/2 \approx 1.1 - 1.6$ eV.
2. What are the effects of O and N defects? Neutral materials have stoichiometries: $Li_{3+x}PO_{4-y}N_z$, with $x = 3z - 2y$. So far we have studied $z = 2y = -x = 1/16$.
   - Stable defect structures
     $\Longrightarrow$ O vacancies cause rebonding of phosphate groups to form bent and straight P−N−P and P−O−P structures.

Further work

- Study effects of defects on Li^+ migration.
- Study other defect structures, such as $x = y = z$ and their effects on interstitial Li^+ migration.
- Simulate properties of glassy structures.